Biochemical control of DNA condensation

Siddharth Agarwal
University of California at Los Angeles
Dino Osmanovic
University of California at Los Angeles
Melissa Klocke
University of California at Los Angeles
Elisa Franco (efranco@seas.ucla.edu)
University of California at Los Angeles https://orcid.org/0000-0003-1103-2668

Article

Keywords: Condensation, phase separation, DNA nanotechnology, strand displacement

Posted Date: June 9th, 2022

DOI: https://doi.org/10.21203/rs.3.rs-1654835/v1

Abstract

Phase separation of molecular condensates is emerging as a key mechanism in biology and biomaterials science. A major advantage of condensates is their capacity to form and reconfigure dynamically, generating responsive compartments that organize molecular targets and reactions in both space and time, in the absence of membranes. While condensation is known to depend on environmental conditions such as temperature and ionic strength, biological condensates in nature are likely influenced by fluctuating biochemical signals with high specificity. Here we ask whether the behavior of artificial condensates can be controlled via chemical reactions by design. Through theory and experiments we examine a model problem in which a phase separating component participates in chemical reactions that activate and deactivate its ability to self-attract. Our theoretical model indicates that such reactions have effects comparable to temperature, and illustrates the dependence of condensate kinetics on reaction parameters. We experimentally realize our model problem through a platform that combines DNA nanostar motifs to generate condensate droplets, and strand displacement reactions to kinetically control the nanostar valency. Our results show that DNA condensate dissolution and growth can be controlled reversibly via toehold-mediated strand displacement, and we characterize the influence of toehold and invasion domains, nanostar size, and nanostar valency. In some cases, the reduction of nanostar valency through invasion stabilizes the droplet size. Our results provide foundational methods for the development of dynamic nucleic acid condensates with potential applications in biomaterials science, nanofabrication, and drug delivery.

Introduction

The discovery of cellular organelles without a membrane has shifted the paradigms of our understanding of life and its origins[1]. These organelles form as molecules in a mixture self-organize into dense, separated compartments, a phenomenon also known as phase separation. An exponentially growing number of studies aims at elucidating the design principles underlying phase separation[2], with the goal of engineering biomolecules that can isolate components and reactions by design, with major implications in biology, biomaterials science, and medicine.

A central question in this context is how biological organisms manage to control the appearance and disappearance of phase separated condensates out of equilibrium. While classically the appearance and disappearance of condensates can be controlled through changes in the temperature and ionic strength, cells must use different mechanisms to form and dissolve organelles over time. Several works have indicated that stoichiometry plays an important role in regulating the emergence of multi-component biological condensates[3,4], suggesting that chemical reactions controlling the abundance of species participating in the condensate are likely to play an important role. These chemical reactions may directly regulate the production or degradation of participating species, or supply chemical agents that can disrupt the multivalent bonds necessary for separation to occur, leading to reversible growth and dissolution of condensates. While it is ideal to test these hypotheses by selectively engineering natural

condensates[5], simplified minimal systems can provide useful biophysical insights while circumventing the native cellular complexity[3,4,6–8]. These systems should offer the possibility to finely control both specific and non-specific interactions among the phase separating components, and the kinetics of chemical reactions that regulate their properties.

DNA nanotechnology is an ideal platform to explore questions pertaining to how chemical reactions can regulate condensate formation. This field has demonstrated that DNA and RNA molecules can be designed to implement chemical reaction networks, self-assembling structures, and amorphous condensates[9,10]. In all these systems, the interactions among nucleic acid domains are prescribed by Watson–Crick–Franklin base-pairing rules, and sequences are designed using computer algorithms[11,12]. DNA structures and complex reactions can include hundreds to thousands of single strands whose programmed domain-level interactions yield the overall desired operation[9]. In addition to designed thermodynamic interactions, DNA nanotechnology also offers methods to control kinetic responses with precision, by taking advantage of strand displacement and branch migration reactions[13]. This coherent design and implementation platform has also enabled the demonstration of systems in which reactions implementing logic or dynamic circuits and self-assembling structures coexist and exchange information for sustained periods of time, with approaches that can be readily extended to couple DNA-based reactions with DNA-based condensates [14–18].

In this article, through theory and experiments we describe a system of condensate droplets whose formation is temporally, reversibly controlled by chemical reactions that activate and deactivate the subunits participating in the condensate. First, we develop a mean field theory of condensates under the impact of chemicals that affect their ability to phase separate, and show how the impact of said chemicals leads to phase diagrams for the system which have similar features to those introduced by changes in temperature. We then apply this theoretical approach to an experimental system in which DNA condensate droplets arise from the sequence-specific interactions of star-shaped DNA motifs known as nanostars[10,19,20]. Using principles from DNA nanotechnology, we demonstrate that droplets can be reversibly grown and dissolved through sequence-specific activation and deactivation of the nanostar bonds. We measure the temporal evolution of droplets size and number under different designs of DNA motifs and reactions, elucidating the dependence of out of equilibrium condensate behavior on various factors under our direction, such as the concentrations of the components involved, their binding affinity, the valency of the nanostars and the size of the nanostars. In particular, we highlight that monomer inhibition is an efficient, ultrasensitive mechanism to control condensate formation, when compared to simply regulating the total concentration of subunits. Our results provide a versatile, minimal DNA-based toolkit for designing and controlling dynamically responsive macroscopic condensates, which may be used to explore fundamental questions in biomolecular phase separation science. This toolset will also enable the synthesis of new biomolecular materials in which the formation of condensates can be temporally and autonomously controlled via a variety of nucleic acid-compatible chemical reactions [21].

Results

A theoretical model suggests means to control condensation through biochemical reactions

The formation of biomolecular condensates depends on many parameters. If we consider an ideal, simplified case in which a single biomolecular species undergoes phase separation, this process is driven primarily by the species concentration and by the temperature of the system, as illustrated by well-understood phase diagrams[22]. However, it is less clear how temporal changes of the concentration of introduced by chemical reactions that deactivate or activate will affect the formation and the kinetics of phase separated condensates, despite recent theoretical work in this area [23,24]

To investigate this problem, we built a mean field model of molecular condensation from the Cahn-Hilliard equation for phase separation in 2D, with the addition of mass action chemical kinetics that introduce temporal changes in the amount of monomers of phase separating species. We consider a case in which elementary chemical reactions convert the monomers between their active form n, which phase separates, and their inactive form n_0, which cannot: an inhibitor molecule I mediates the deactivation of monomers, while an activator mediates their reactivation by removing inhibitor, a process that generates waste *W*:

$$n + I \underset{k_b}{\overset{k_f}{\rightleftharpoons}} n_0 \qquad n_0 + A \underset{k_b}{\overset{k_f}{\rightleftharpoons}} n + W$$

The full derivation of the mean field equations, along with a description of their computational integration, is in Section 4.1 of the Supplementary Information (SI) file. First, we note that the stationary effect of including inhibitor species in the system is similar to a change in temperature, as evidenced by phase diagrams obtained under different dissociation constants (SI Fig. S62). Next, we perform computational simulations exploring the system's kinetic response to the introduction of inhibitor and activator.

Figure 1A illustrates the behavior of a system in which droplets are allowed to phase separate first, with later sequential addition of inhibitor and activator at different ratios (.25x, .5x and 1x the level of monomer). These computationally generated images qualitatively confirm that addition of inhibitor causes droplet dissolution, and addition of activator promotes their regrowth. From these images, we gathered quantitative insight on the evolution of droplet size over time (normalized relative to the forward binding rate and the monomer concentration).

After addition of inhibitor, the half time for dissolution of individual droplets scales with a power law of the droplet radius (Fig. 1B), meaning that larger droplets take longer to dissolve. In contrast, the droplet ensemble dissolves faster when the total droplet surface is larger (Fig. 1C), i.e. when the monomers are allowed to phase separate for a longer period of time prior to adding inhibitor. Consistent with expectation, the average droplet size decreases faster when the inhibitor to monomer ratio is larger (Fig. 1D). This process is however affected by the inhibitor diffusion rate (), which manifests as a change in the temporal scaling law when the diffusion constant is between 1 and 10 (Fig. 1E). This indicates that

inhibition may be surface-driven (slower diffusion), or volume driven (faster diffusion). Overall, increasing either the inhibitor concentration or its diffusion coefficient promotes faster droplet dissolution, though apparently with different scalings.

The addition of activator (in stoichiometric amount to the inhibitor) promotes droplet regrowth. However, Fig. 1F shows that the speed of regrowth depends on both the initial droplet size and on the activator to monomer ratio. If we focus on the average droplet area, we note a rapid increase at 0.25 and 0.5x ratios; in contrast, a slow increase is noticeable at a 1x ratio. This non-monotonic behavior emerges due to the presence of three processes driving growth: monomer activation, droplet nucleation, and droplet coarsening. When a large number of monomers are rapidly activated (Fig. 1A, post addition of 1x activator) nucleation of new, small droplets dominates over the coarsening of existing ones, resulting in slower increase of their mean size. As one would anticipate, the diffusion rate of the activator does not significantly influence droplet growth (Fig. 1G).

This simple theoretical model establishes a baseline expectation for the temporal behavior of droplets and for the degree of controllability of their average size. To test these expectations, we next develop an experimental platform to build dynamic biomolecular condensates using DNA nanotechnology.

The formation of DNA condensate droplets can be controlled via strand displacement

We used synthetic DNA motifs and strand displacement as a platform to probe the effects of chemical reactions on the condensation of droplets. We adopted multiarm DNA motifs, or DNA nanostars, that interact via complementary palindromic ‘sticky-end’ (SE) domains present on the end of each arm[10,19,20]. We started our investigation with three-arm motifs (valency equal to three) characterized by Sato et al.[20], each arm having a four-base sticky-end, shown in Fig. 2A. After assembly by thermal annealing the nanostars can be considered monomers that spontaneously yield DNA-rich condensed droplets, which in our case are expected to remain liquid at room temperature (27°C) while coarsening and coalescing into larger droplets[20]. Nanostars were annealed at 5 μM concentration unless otherwise noted. To monitor the condensate droplets via fluorescence microscopy, we modified one of the strands of the nanostars to include a fluorescent dye (Cy3).

To control the growth and dissolution of droplets, we designed DNA species with the capacity to react with the nanostars, specifically to switch the state of their sticky-ends between inactive and active. To enable the inactivation of nanostars, we designed a strand displacement reaction controlling the availability of one of the sticky-ends: we reasoned that a reduction of the valency from three to two would be sufficient to dissolve the DNA-dense droplets. To make it possible to deactivate one sticky-end, we modified it to include a 7 nucleotide (nt) ‘toehold’ domain that is designed to have no secondary structure and to remain single-stranded (Fig. 2A and 2B). The toehold enables strand invasion by a DNA inhibitor molecule, henceforth dubbed ‘invader’, designed to be complementary to the toehold, the sticky-end

sequence, and 6 nt of the nanostar arm. While an invader can weakly interact with any unpaired sticky-end and arm on the nanostars, it cannot invade base-paired sticky-ends that do not have a toehold.

To allow for nanostar activation, the invader molecules are in turn designed to include their own toehold domain (6 nt), so that a complementary 'anti-invader' (AI) strand can displace invader bound to a nanostar. This displacement reaction releases the sticky-end of the nanostar, which recovers its original valency and its capacity to yield condensate droplets. Invader and anti-invader serve the purpose of activating and deactivating nanostar units via chemical reactions that are equivalent to those described in our theoretical model.

After forming condensate droplets with our toeholded DNA nanostars, we sequentially added invader and anti-invader at equimolar levels relative to the nanostar concentration, and characterized the droplets kinetics during each reaction. Before starting invasion and anti-invasion, we annealed the DNA nanostars at a concentration of 5 μM and allowed the samples to grow at 27°C for 30 mins, measuring a coefficient of variation of 0.12 for droplet diameter, 0.23 for area, and 0.005 for number across three experimental replicates. These statistics set a baseline for the significance of differences observed across kinetic droplet experiments that have a significant dependence on initial conditions, as illustrated in our theoretical example. Example fluorescence microscopy images of condensates before invasion, after invasion and after anti-invasion are shown in Fig. 2C. The microscopy images were used to gather statistics of the condensate droplet diameter as a function of time, shown in the histograms in Fig. 2C (our methods for image processing are described in SI Section 2.5). The addition of invader causes condensates to disappear within two minutes (addition of a scramble sequence has no effect on the droplets, Fig S6), indicating that the dissolution time-scale is driven by the rapid forward rate of strand invasion. In contrast, droplet regrowth after the addition of anti-invader is a slow process driven by nucleation, coarsening, and coalescence of droplets.

The concentration of invader and anti-invader determine the kinetics of droplet dissolution and formation.

The kinetics of droplet dissolution and formation should depend on the level of inhibiting (invader) and activating (anti-invader) molecules relative to the level of monomer (nanostar), as anticipated by our simple model (Fig. 1D). To quantify this dependence we measured the average droplet area over time after sequential addition of invader and anti-invader (AI). The area was normalized relative to its initial value prior to initiating invasion and anti-invasion (Fig. 2D). Like the model predicts, the time it takes to dissolve droplets decreases monotonically with the invader to monomer ratio, with 1X invader resulting in droplet dissolution within two minutes, and 0.5X invader dissolving droplets in 15 minutes. However, a 0.25X level of invader only reduces the average droplet size without causing their complete dissolution. In contrast, the regrowth kinetics after addition of AI do not monotonically scale with the amount of AI, as anticipated by our model (Fig. 1F). A 0.5X amount of AI (equimolar to 0.5X invader added) yields a significantly faster regrowth of droplets. The 0.25X and 1X experiments produce a slower regrowth, albeit

presumably for different reasons: at 0.25X, slow coarsening is likely the driving process, while at 1X the rapid activation of a large number of monomers makes nucleation of small droplets the dominant process (which yields an overall smaller average size). The addition of excess AI either does not significantly change (2X relative to nanostar level) or suppresses (4X) droplet regrowth (Fig. 2E). This can be explained by the fact that the AI sequence includes the 4-base palindromic domain of the nanostar sticky-ends, making it possible for the AI to associate with nanostars and prevent their separation, an effect that becomes predominant when AI is present in excess.

Given that droplets rapidly dissolve and reform upon addition of 0.5X invader and AI, we asked whether their addition in multiple, sequential cycles would yield similar results. Figure 2F shows six separate cycles of invasion, and anti-invasion: invader and AI added in each cycle bind and form a fully double stranded ‘waste’ species that accumulates over time but is expected to be inert. Incorporation of inert waste in the condensates may be the reason why cycles 5 and 6 show a more pronounced regrowth. Overall, these results show that toehold-mediated strand displacement, a programmable biochemical reaction, can be used to direct self-assembly of large DNA condensates isothermally and reversibly, by activating and deactivating the motifs participating in the condensation process.

Valency reduction is a high-gain mechanism to control condensate kinetics

The observation that only 0.5X invader results in complete droplet dissolution prompted us to examine more carefully the influence of concentration of active DNA nanostars on their capacity to phase separate. Because high nanostar concentrations were adopted in previous work (typically 5 μM), we tested whether condensation is at all possible at lower nanostar concentrations, with an expectation that no condensation would occur below 2.5 μM (the level of active nanostars remaining after addition of 0.5X invader in our experiments). In contrast, we found that droplet condensates form at concentrations as low as 0.25 μM. Figure 3A (orange) reports the normalized total droplet area 30 minutes after annealing for separate experiments with nanostars at 0.25 μM, 1 μM, 2.5 μM, and 5 μM, and Fig. 3B reports normalized average area and Fig. 3C reports normalized droplet number (areas are normalized relative to the 5μM measurement). These results indicate that in our invasion experiments, dissolution of droplets is not due to the fact that the concentration of active nanostars in solution is brought below their critical threshold for condensation.

To further investigate this, we monitored the formation of droplets when 5μM DNA nanostars are annealed in the presence of invader (.25X to .5X). The normalized total droplet area 30 minutes after anneal is shown in Fig. 3A (dark red) versus the concentration of active nanostar, calculated as the difference between their total concentration and the concentration of invader. Average area and number are in Fig. 3B and Fig. 3C (dark red). These graphs make it possible to compare two distinct series of experiments that have the same amount of active monomers, but one includes invader and the other does not. In the presence of invader, samples include smaller and more numerous droplets, and condensation is completely suppressed by reducing the valency of only 1/2 the nanostar population. In

contrast, in the absence of invader condensation may be suppressed with a reduction of more than 1/20 the nominal nanostar concentration (5μM).

Overall, this comparison indicates that using invader to reduce nanostar valency yields more than 2x “gain” toward suppressing condensation, as qualitatively suggested by the slope of the graphs in Fig. 3A. This behavior can be regarded as ultrasensitive, in that condensate formation is triggered under a small increment of the concentration of active monomers exceeding half the total. The fact that only half of the nanostar population requires deactivation for droplet dissolution prompts us to suggest a model in which inactive nanostars (valency two) interact with active ones, sequestering them and reducing the critical concentration for phase separation (Fig. 3E). In other words, a single invasion event affects multiple nanostars resulting in the observed “gain”.

This behavior can be captured with a theoretical model by performing linear stability analysis around the stationary state under different condition concentrations of inactivated nanostar and net attraction to the activated nanostar (SI Section 4.1). This stability analysis yields the phase diagram in Fig. 3D and indicates that there are conditions where the presence of inactivated nanostars alone is sufficient to disrupt the formation of condensates. It does this by raising the free energy of the droplet state relative to the disperse state. The theory predicts this behavior even in the absence of any chemical reactions, suggesting a thermodynamic origin of this phenomenon. Theoretically, this suggests that if the inactivated nanostars are not strongly excluded from the droplet, they will diffuse into the droplet, thus reducing the relative energetic benefit of the droplet existing by interrupting the multivalent droplet interactions, leading to droplet dissolution.

Droplet size can be controlled by modifying invasion and anti-invasion domains

We next tested how changes in the forward rate of invasion affect the dissolution of droplets. As is well-known from methods in DNA nanotechnology, the speed of strand displacement (forward rate) depends on the length of the toehold domain, so we designed nanostar variants (and corresponding invaders) with a toehold of 5 and 3 nucleotides, and one variant without a toehold (Fig. 4A). The speed of invasion should scale exponentially with the reduction of toehold length[25], but invaders (1X) with shorter toeholds yield dissolution that is only marginally slower (Fig. 4B). A drastic shift in the behavior of the droplets occurs when the toehold domain is eliminated: in this case, droplets do not dissolve but their average size remains constant over 6 hours/360 mins post addition of invaders; also the number of droplets shows limited change over time (SI Section 3.6). We expect the invader weakly binds and unbinds to the free (unpaired) sticky-ends of the nanostars, that may be in solution or on the surface of the condensate droplets, thereby slowing down coarsening and fusion events (the nanostar arm-invader interaction domain is the same as a nanostar-nanostar arm interaction). Without a toehold, the invader may be considered a “decoy” molecule that stabilizes condensates.

While the toehold length affects the forward kinetics of invasion, the overall complementarity of invader-nanostar arm sequences determines the stability of the complex they form. The effects of this design

parameter on the behavior of droplets is reported in Fig. 4D, that compares invader variants including 9, 6, 3 (nominal case shown in Fig. 2), and 0 nt complementary to the arm sequence. At 0.5X invader level, all the variants dissolve droplets within 15 minutes, indicating that invasion depth is not a major driver of droplet dissolution kinetics. In contrast, there is a significant difference in the anti-invasion behavior when comparing the variants with 0, 3 nt depth and those with 6, 9 nt depth (0.5X AI fully complementary to invader). Shorter variants yield droplets that regrow slowly, and do not exceed 30% their original average area. This is likely due to interactions between the nanostar and the AI, which can yield kinetically trapped complexes including nanostar, invader, and AI, which are equivalent to inactive nanostars.

The speed of droplet dissolution depends on the size of DNA nanostars.

Our theoretical model predicts that dissolution speed depends on the diffusion rate of the inhibitor molecule (Fig. 1D). To test whether we could change the diffusion of invader into the condensate, and thus droplet dissolution speed, we varied the length of nanostar arms between 8 and 24 base pairs (bp) in Fig. 1A. Because we considered arm lengths well below the persistence length of double stranded DNA (50 bp), it is reasonable to expect that longer arms yield droplets that are less densely packed and more permeable to invaders.

We first verified that all variants form droplets in the absence of a toehold, with 8 bp arm nanostars yielding noticeably smaller droplets than the 24 bp arm variant post anneal, as we found in recent work[26]. However, the 24 bp arm design did not yield droplets in the presence of a 7 nt toehold (similarly, 32 bp arm nanostars did not condense in the presence of any toehold; SI Fig. S34). For this reason, in all variants we adopted a 3 nt toehold, which in the nominal 16 bp arm design promoted droplet dissolution within 15 minutes at 1X invader (Fig. 4B).

At 1X invader level, droplets generated by all variants dissolve within 15 minutes: Fig. 5B reports normalized droplet average area versus number, parameterized with respect to time (time points are associated with markers). Following the arrow on each trace, the droplet number sharply decreases by 80–90% the initial level within 2 minutes, with few large droplets persisting for the 16 and 24 base design. The 8 bp variant dissolves significantly faster.

At 0.5X invader level, droplets in the 8 bp arm variant take about 20 minutes to dissolve, with droplet number and size gradually decreasing, as shown in Fig. 5C. Droplets in the 16 and 24 bp arm variants decrease in number, but their average area increases relative to the initial conditions (by 40% and 20% respectively). Over time, large droplets persist in the 16 bp arm design; while we observe minor change in their number, droplet average area fluctuates significantly, likely because few large droplets are captured per field of view (example images in Fig. 5D). Over time droplets persist also in the 24 bp arm variant, but their average size is around half the initial, with more significant fluctuations in their number. Notably, after 24 hours, droplets from 16 and 24 bp variants grow well above their initial average. Additional

images and data (diameter histograms, average and total droplet area, and droplet number) are in SI Section 3.7.

These experiments do not indicate a clear correlation between nanostar size and invasion speed, suggesting that diffusion rate of invader may not significantly differ in the size range we considered. However, our theoretical model predicts that the time it takes a droplet to disappear depends on its radius as $R^{3/2}$, and by making the nanostars smaller, we reduce the radii of the droplets [26]. However, we increase the concentration of invadable sticky-ends inside droplets (which also decreases the time taken for a droplet to dissolve by rescaling the time). The competition of these effects together suggest that the time taken for droplets of smaller nanostars to dissolve would be faster, as is indeed observed in experiment.

Selective control of monomer valency via individually addressable toeholds results in distinct dissolution behaviors

The valency of DNA nanostar motifs is determined by the number of arms, a parameter that is known to affect the phase diagram of the system [10,19,20]. Here we demonstrate that, like three-arm nanostars considered so far, nanostars with higher valency can be controlled by strand invasion reactions that target specific toehold domains. Further, we investigate the kinetics of droplet dissolution as valency is progressively reduced by invader binding.

Nanostars with 4 and 6 arms, presenting distinct sequences in each arm but identical palindromic 4 nt sticky-ends, were engineered to include a variable number of 7 nt toeholds, each characterized by a distinct sequence (schematics in Fig. 6A and C). We then designed a set of invaders, each complementary to a single specific toehold and arm, so that individual arms on a nanostar can be selectively deactivated. For these experiments, we used stoichiometric amounts (1X) of each invader with respect to the nanostar level, to deactivate all the corresponding sticky ends and fully reduce the motif valency.

For the 4 arm motif, we found that the invasion of a single sticky-end is sufficient to dissolve droplets within 15–20 minutes, causing a 90% drop in the number of droplets detected within 2 minutes. The invasion of two sticky-ends accelerates dissolution, which is complete in under 5 minutes (Fig. 6A and B). Removal of invaders by their specific anti-invader results in droplet regrowth (SI Section 3.9).

For the 6 arm motif, invasion of a single sticky-end is insufficient to completely dissolve droplets, however their number is reduced by 70–80% and their average size by 60% over the course of two hours of observation. Invasion of two sticky-ends reduces the droplet number by more than 70% in five minutes, however the droplet average size decreases very slowly, reaching 30% the initial size over two hours of observation. Invasion of 3 adjacent sticky-ends is necessary to completely dissolve the droplets, with over 90% of droplets dissolved in the first 5 minutes, and the remaining larger droplets requiring about two hours to be eliminated. In contrast, invading three staggered sticky-ends yields a droplet dissolution

behavior comparable to the invasion of two adjacent sticky-ends. (After 24 hours, the staggered three arm design shows very large droplets, see SI Fig. S59). These results suggest that orientational order of the nanostar arms is important for condensation. If the remaining active arms cannot easily connect in a tessellating pattern, formation of condensates becomes more difficult.

Programmable dynamic control of dissolution and formation of distinct coexisting condensates

A major advantage of DNA nanotechnology is the possibility to build motifs and assemblies that are structurally identical but operate as orthogonal, non-interacting species. This principle can be extended to the design of motifs yielding condensates[20,27], and to the strand displacement reactions that control them. To illustrate this advantage, we designed two orthogonal 3 arm DNA nanostars with different sticky-ends, and labeled them with distinct fluorophores (Nanostar 1, Cy3; and Nanostar 2, FAM; shown in Fig. 7). As DNA backbones are negatively charged, DNA nanostars do not spontaneously interact in the absence of base-pairing. To minimize the interactions between palindromic SEs of the two designs, nanostars were designed to have 6 nt sticky-ends. (Notably, palindromic 4 nt sticky-ends containing only ‘A’s and ‘T’s do not yield condensates, see also SI Fig S60). The use of 6 nt sticky-ends however is expected to raise the temperature at which the condensates transition from a liquid to a gel state as noted in the literature[20,28]. This is confirmed by the fact that even though invasion yields droplet dissolution at room temperature within a few minutes, we were unable to regrow these condensates even after 3 hours of anti-invader addition (SI Fig S61). By raising the temperature to 34°C, we were able to recover reversible phase transitions using invader and anti-invader.

The two nanostar types were annealed in the same pot, producing condensates of distinct colors, orange for Nanostar 1, labeled with Cy3, and green for Nanostar 2, labeled with FAM. The droplets remained demixed, and were not observed to fuse (Fig. 7, left). We then split the sample in two: we added sequentially the invader (1X) and the anti-invader (1X) designed for Nanostar 1 to the first aliquot, observing complete dissolution and then regrowth of the orange droplets, while the distribution of green droplets is qualitatively unaffected (Fig. 7, top row of images). Similarly, when invader and anti-invader for Nanostar 2 were sequentially added, we observed dissolution and regrowth of the green droplets, while the orange ones remained intact.

These results demonstrate the design of two orthogonal artificial DNA condensates that are dynamically controllable via tailored chemical reactions, and we expect they can be easily scaled to systems in which dozens of distinct condensates are individually addressable by sequence-specific DNA or RNA regulators.

Discussion And Conclusion

All forms of life require the presence of physically separated compartments that isolate molecules and reactions, enhancing or limiting their functions. Similarly, artificial materials can achieve life-like behaviors by combining the operation of distinct functional partitions. In both contexts, condensation is a key mechanism to self-organize molecules in the absence of membranes[21,29]. An important characteristic

of condensates is that they form and dissolve dynamically, shuttling guest molecules across distinct phases. Learning how to control these dynamic properties via biochemical reactions, under homeostatic conditions, will make it possible to build complex molecular systems and materials that self-organize in space and time, provide insights on similar phenomena in biological cells, and possibly offer hypotheses on how life originated[30].

Through theory and experiments, we have defined a model problem to elucidate how chemical reactions can achieve dynamic control over condensation. We have considered a phase separating species that is sequentially inhibited or activated via reactions that turn on or off its ability to condense. First, we have set up a computational model that sets up expectations for the thermodynamic and kinetic behavior of condensate droplets under different concentrations of inhibitor and activator, reaction rate constants, and diffusion rates. Next, we have realized this model problem through a platform of DNA components that implement both a phase separating process and the chemical reactions that regulate it. We achieved this by engineering DNA nanostars, a versatile motif that generates phase separated condensates depending on the number of arms and on the sequence of their sticky-ends, that determine the valency and bond stability of the nanostars[19,20]. Three-arm nanostars were modified to include a toehold that allows for sequence-specific strand invasion of one of the nanostar arms by an invader DNA strand. By reducing the nanostar valency, the invader inhibits nanostar phase separation and dissolves the droplets. Displacement of the invader via an anti-invader strand results in re-activation of the nanostars, and regrowth of droplets. Our study focuses exclusively on phase separation induced by chemical reactions, although separated droplets may experience transitions between liquid and gel that could be studied via rheology experiments falling outside of the scope of this paper.

We have shown that condensates can be regulated by chemical inputs that change the balance of the phases leading to shrinking or growth. Following on this, we can broadly identify two different mechanisms of control over condensation through inhibitors, which we deem *thermodynamic* and *chemical.* In thermodynamic control, a system close to the transition point can be pushed across the phase separation boundary, leading to a region in phase space where the dispersed phase is favored. This could proceed exclusively via sequestration of monomers in the dispersed phase, leading to a thermodynamic phase transition where the droplets slowly lose material through thermal fluctuation. Chemical control, by contrast, proceeds via the deactivation of the monomers in both the dispersed and the dense phase, as monomers participate in chemical reactions. While our experiments focused on establishing means for chemical control, the response of our system is due to the simultaneous presence of thermodynamic and chemical control. For example, Fig. 3 shows that an amount of inhibitor that is insufficient to deactivate all the monomers can still lead to complete dissolution of the droplets, because a mix of activated and deactivated momoners presents a different phase diagram when compared to active monomers alone.

The dynamic condensates we built using DNA nanotechnology show unexpected behaviors that may be generalizable to other biomolecular condensates. First, we have found that valency reduction induces complete or partial condensate dissolution in all cases considered. In trivalent nanostars, this reaction

has an effect comparable to a sharp increase of the critical concentration threshold for condensation, indicating that valency reduction is an efficient mechanism to control phase separation. This finding may be significant biologically, as it points to the possibility that the size and number of biomolecular condensates may be controlled rapidly by regulators that interact with a fraction of phase separating monomers, whose total mass may be conserved. This is reminiscent of the operation of phosphorylation pathways, which transmit signals by activating and deactivating their protein targets on timescales much faster than protein production and degradation. We also observed that the interactions among invaders and nanostars can in some cases stabilize the condensate size and number, a yet to be explained phenomenon that may be due to a combination of factors including changes of the condensate surface[31]. Finally, through engineering nanostars with different placements of invasion toeholds, we demonstrated that the orientation of the remaining active arms plays a significant role in the formation of condensates. This information could be used to customize DNA condensates not only to achieve prescribed thermodynamic and kinetic properties, but also to introduce domains that harbor particular functions, like recruiting guest molecules or performing catalytic reactions[32,33] .

Our work builds on many recent demonstrations of responsive DNA-based soft materials. Entangled DNA strands, linear cross-linked motifs, and nanostars have been engineered to generate hydrogels with tunable mechanical and rheological properties[19,34]. Dynamic responses in DNA hydrogels have been obtained by using strand displacement, for example to control DNA hydrogel stiffness[35], to program swelling[36], and to introduce re-entrant behaviors[37]. Further, by integrating specific DNA motifs, DNA-based hydrogels can be made responsive to a variety of chemical and physical stimuli, including enzymatic reactions, pH, light, and temperature [34]. Similarly, DNA condensates may be designed to respond dynamically to many types of inputs, as recently illustrated by studies of their enzymatic degradation[38]. Orthogonal sequence design has been used previously to build condensates that coexist without mixing [20,27], a behavior that we were able to reproduce here. These results may be systematically expanded to produce libraries of DNA or RNA condensates that can be selectively grown and dissolved.

The dynamic condensates described here inherit the programmability of systems previously demonstrated by DNA nanotechnology[9], and could be coupled with a variety of other DNA devices. DNA condensates could be designed to respond to multiple inputs and complex chemical reactions through the expanding number of modular sensors, logic circuits, and dynamic circuits based on strand displacement[13]. Molecular instructions may even include algorithmic or dynamic behaviors, like demonstrated in crystalline DNA structures[16,39,40]. Finally, responsive nucleic acid condensates like those described here may be used as scaffolds to other materials[41], or to localize molecules and reactions on demand[42,43], expanding the toolkit of DNA and RNA materials for the advancement of artificial life, synthetic biology, and biotechnology applications.

Declarations

Acknowledgements

This research was supported by NSF through CAREER award 1938194 and FMRG: Bio award 2134772 to EF, and by the Sloan Foundation through award G-2021-16831. We thank Deborah Fygenson, Paul Rothemund, Eli Kengmana, and Rebecca Schulman for helpful advice and feedback.

References

1. Banani, S. F., Lee, H. O., Hyman, A. A. & Rosen, M. K. Biomolecular condensates: organizers of cellular biochemistry. *Nat. Rev. Mol. Cell Biol.* **18**, 285–298 (2017).

2. Hyman, Anthony A. , Christoph A. Weber, and Frank Jülicher. Liquid Liquid Phase Separation in Biology. *Annual Review of Cell and Developmental Biology* **30**, 39–58 (2014).

3. Banani, S. F. *et al.* Compositional Control of Phase-Separated Cellular Bodies. *Cell* **166**, 651–663 (2016).

4. Boeynaems, S. *et al.* Spontaneous driving forces give rise to protein-RNA condensates with coexisting phases and complex material properties. *Proc. Natl. Acad. Sci. U. S. A.* **116**, 7889–7898 (2019).

5. Zhang, H. *et al.* RNA Controls PolyQ Protein Phase Transitions. *Mol. Cell* **60**, 220–230 (2015).

6. Alshareedah, I., Moosa, M. M., Raju, M., Potoyan, D. A. & Banerjee, P. R. Phase transition of RNA-protein complexes into ordered hollow condensates. *Proc. Natl. Acad. Sci. U. S. A.* **117**, 15650–15658 (2020).

7. Aumiller, W. M., Jr, Pir Cakmak, F., Davis, B. W. & Keating, C. D. RNA-Based Coacervates as a Model for Membraneless Organelles: Formation, Properties, and Interfacial Liposome Assembly. *Langmuir* **32**, 10042–10053 (2016).

8. Deng, J. & Walther, A. Programmable ATP-Fueled DNA Coacervates by Transient Liquid-Liquid Phase Separation. *Chem* vol. 6 3329–3343 (2020).

9. Seeman, N. C. & Sleiman, H. F. DNA nanotechnology. *Nature Reviews Materials* vol. 3 (2018).

10. Biffi, S. *et al.* Phase behavior and critical activated dynamics of limited-valence DNA nanostars. *Proc. Natl. Acad. Sci. U. S. A.* **110**, 15633–15637 (2013).

11. Zadeh, J. N. *et al.* NUPACK: Analysis and design of nucleic acid systems. *J. Comput. Chem.* **32**, 170–173 (2011).

12. Douglas, S. M. *et al.* Rapid prototyping of 3D DNA-origami shapes with caDNAno. *Nucleic Acids Research* vol. 37 5001–5006 (2009).

13. Simmel, F. C., Yurke, B. & Singh, H. R. Principles and Applications of Nucleic Acid Strand Displacement Reactions. *Chemical Reviews* vol. 119 6326–6369 (2019).

14. Agarwal, S. & Franco, E. Enzyme-Driven Assembly and Disassembly of Hybrid DNA-RNA Nanotubes. *J. Am. Chem. Soc.* **141**, 7831–7841 (2019).

15. Schaffter, S. W., Scalise, D., Murphy, T. M., Patel, A. & Schulman, R. Feedback regulation of crystal growth by buffering monomer concentration. *Nat. Commun.* **11**, 6057 (2020).

16. Green, L. N. *et al.* Autonomous dynamic control of DNA nanostructure self-assembly. *Nat. Chem.* **11**, 510–520 (2019).

17. Zhang, D. Y., Hariadi, R. F., Choi, H. M. T. & Winfree, E. Integrating DNA strand-displacement circuitry with DNA tile self-assembly. *Nat. Commun.* **4**, 1965 (2013).

18. Agarwal, S., Klocke, M. A., Pungchai, P. E. & Franco, E. Dynamic self-assembly of compartmentalized DNA nanotubes. *Nat. Commun.* **12**, 3557 (2021).

19. Conrad, N., Kennedy, T., Fygenson, D. K. & Saleh, O. A. Increasing valence pushes DNA nanostar networks to the isostatic point. *Proceedings of the National Academy of Sciences* vol. 116 7238–7243 (2019).

20. Sato, Y., Sakamoto, T. & Takinoue, M. Sequence-based engineering of dynamic functions of micrometer-sized DNA droplets. *Sci Adv* **6**, eaba3471 (2020).

21. Liu, A. P. *et al.* The living interface between synthetic biology and biomaterial design. *Nat. Mater.* **21**, 390–397 (2022).

22. Safran, S. A. *Statistical thermodynamics of surfaces, interfaces, and membranes*. (CRC Press, 2018).

23. Weber, C. A., Zwicker, D., Jülicher, F. & Lee, C. F. Physics of active emulsions. *Rep. Prog. Phys.* **82**, 064601 (2019).

24. Zwicker, D., Seyboldt, R., Weber, C. A., Hyman, A. A. & Jülicher, F. Growth and division of active droplets provides a model for protocells. *Nat. Phys.* **13**, 408–413 (2016).

25. Yurke, B. & Mills, A. P. Using DNA to power nanostructures. *Genet. Program. Evolvable Mach.* **4**, 111–122 (2003).

26. Agarwal, S., Osmanovic, D., Klocke, M. A. & Franco, E. The growth rate of DNA condensate droplets increases with the size of participating subunits. doi:10.1101/2022.03.29.486311.

27. Jeon, B.-J., Nguyen, D. T. & Saleh, O. A. Sequence-Controlled Adhesion and Microemulsification in a Two-Phase System of DNA Liquid Droplets. *J. Phys. Chem. B* **124**, 8888–8895 (2020).

28. Xing, Z. *et al.* Microrheology of DNA hydrogels. *Proc. Natl. Acad. Sci. U. S. A.* **115**, 8137–8142 (2018).

29. Alberti, S. Phase separation in biology. *Current Biology* vol. 27 R1097–R1102 (2017).

30. Earth, I. S. on T. O. of L. on T., International Symposium on the Origin of Life on the Earth & Oparin, A. I. Proceedings. Edited for the Academy of Sciences of the U.S.S.R. by A.I. Oparin [and others]. (1959) doi:10.5962/bhl.title.10222.

31. Nguyen, D. T., Jeon, B.-J., Abraham, G. R. & Saleh, O. A. Length-Dependence and Spatial Structure of DNA Partitioning into a DNA Liquid. *Langmuir* **35**, 14849–14854 (2019).

32. Kojima, T. & Takayama, S. Membraneless Compartmentalization Facilitates Enzymatic Cascade Reactions and Reduces Substrate Inhibition. *ACS Appl. Mater. Interfaces* **10**, 32782–32791 (2018).

33. O'Flynn, B. G. & Mittag, T. The role of liquid-liquid phase separation in regulating enzyme activity. *Curr. Opin. Cell Biol.* **69**, 70–79 (2021).

34. Bush, J., Hu, C.-H. & Veneziano, R. Mechanical Properties of DNA Hydrogels: Towards Highly Programmable Biomaterials. *Applied Sciences* vol. 11 1885 (2021).

35. Yue, L., Wang, S., Wulf, V. & Willner, I. Stiffness-switchable DNA-based constitutional dynamic network hydrogels for self-healing and matrix-guided controlled chemical processes. *Nat. Commun.* **10**, 4774 (2019).

36. Fern, J. & Schulman, R. Modular DNA strand-displacement controllers for directing material expansion. *Nat. Commun.* **9**, 3766 (2018).

37. Bomboi, F. *et al.* Re-entrant DNA gels. *Nat. Commun.* **7**, 13191 (2016).

38. Saleh, O. A., Jeon, B.-J. & Liedl, T. Enzymatic degradation of liquid droplets of DNA is modulated near the phase boundary. *Proc. Natl. Acad. Sci. U. S. A.* **117**, 16160–16166 (2020).

39. Petersen, P., Tikhomirov, G. & Qian, L. Information-based autonomous reconfiguration in systems of interacting DNA nanostructures. *Nat. Commun.* **9**, 5362 (2018).

40. Rothemund, P. W. K., Papadakis, N. & Winfree, E. Algorithmic self-assembly of DNA Sierpinski triangles. *PLoS Biol.* **2**, e424 (2004).

41. Kurokawa, C. *et al.* DNA cytoskeleton for stabilizing artificial cells. *Proc. Natl. Acad. Sci. U. S. A.* **114**, 7228–7233 (2017).

42. Jain, A. & Vale, R. D. RNA phase transitions in repeat expansion disorders. *Nature* **546**, 243–247 (2017).

43. Leathers, A. *et al.* Reaction-diffusion patterning of DNA-based artificial cells. doi:10.1101/2022.03.24.485404.

Figures

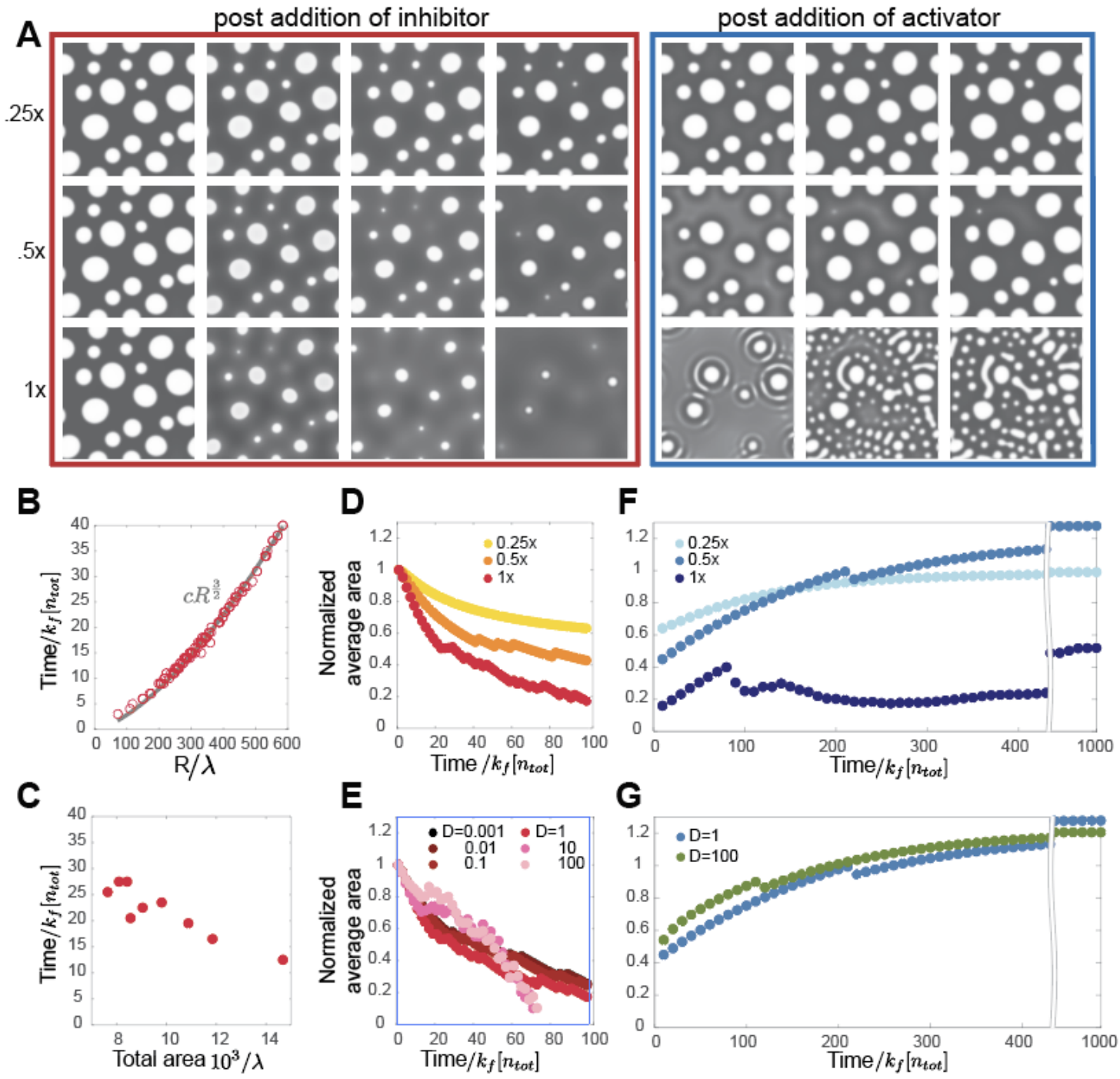

Figure 1

A computational model illustrates the effects of inhibition and activation chemical reactions on phase separated droplets. *A) Computationally generated images of droplets. We combined the Cahn-Hilliard*

equation for phase separation with chemical reactions: an inhibitor deactivates the phase separating material, causing droplets to shrink over time; droplets regrow after addition of activator. B) The half time until a droplet reaches half its size scales to the 3/2 power of the perimeter of the droplet. C) The half time decreases when a larger total surface is present. Parameter λ represents the length scale associated with the surface tension D) Droplets dissolve faster at higher inhibitor levels. E) Average droplet area over time, at different inhibitor diffusion constants D. We identify a slow regime, (surface driven) in which as the surface decreases in time, the time taken for the droplet to dissolve will increase, leading to a slowing down of dissolution in time. The opposite is the case for inhibitors diffusing fast. F) Average droplet area after addition of different amounts of activator. G) Regrowth does not depend on the activator diffusion constant.

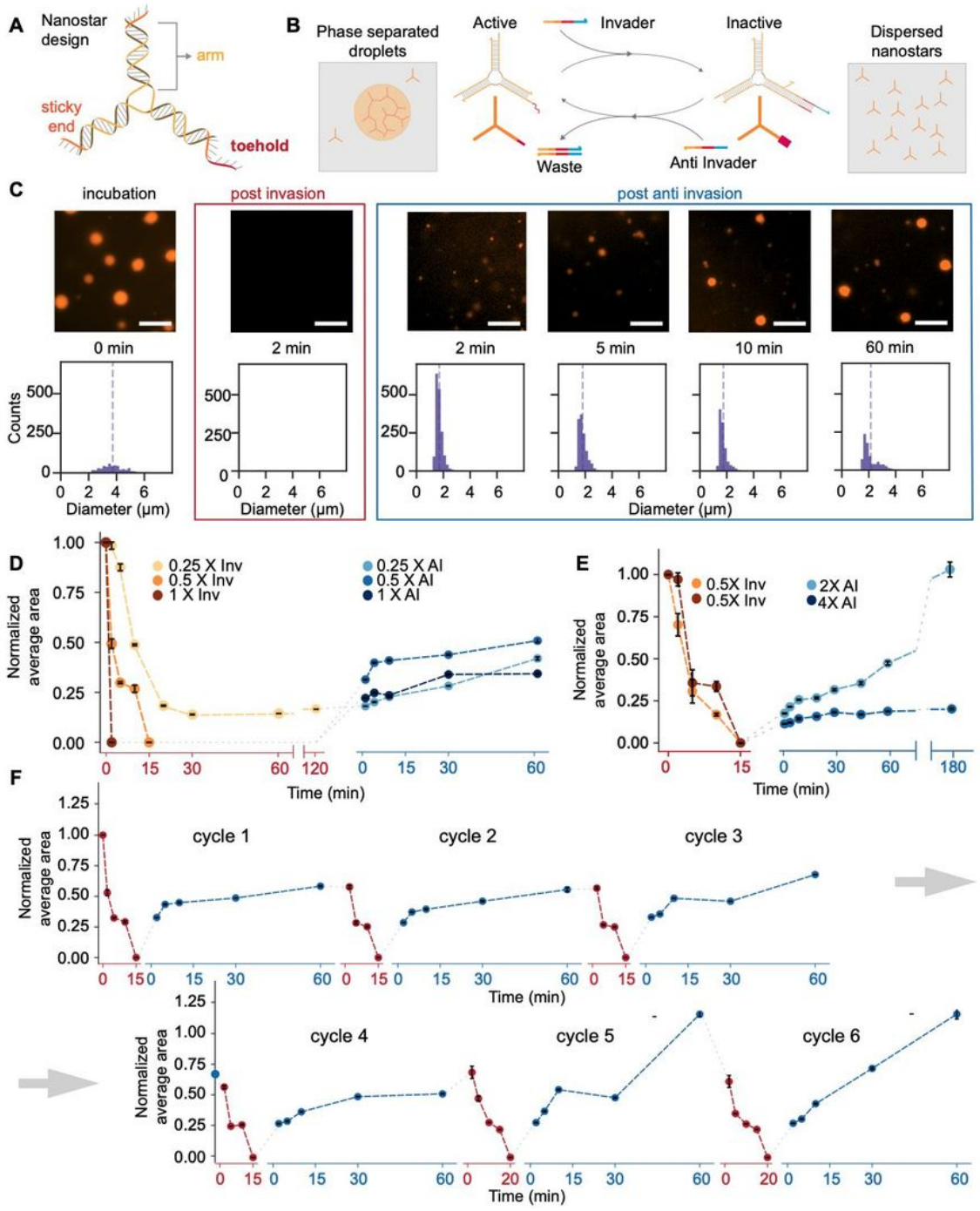

Figure 2

Controlling condensation of DNA motifs over time via strand displacement reactions. *A) Schematic of 3-arm DNA nanostar. One of the nanostar sticky-ends was modified to include a single-stranded overhang, or toehold (red domain on the 5' end of one arm). B) Schematic of the chemical reactions of invasion and anti-invasion for controlling the capacity of nanostars to yield phase separated droplets. C) Representative microscopy images of condensate droplets before invasion, post invasion and post anti-*

invasion, and histograms of condensate diameter. D) Normalized average area of droplets during invasion and anti-invasion reactions for different concentrations of invader and anti-invader. E) Excess of anti-invader limits droplet regrowth due to weak interactions with the nanostar sticky-ends. F) Invasion and anti-invasion reactions can be sequentially repeated multiple times (bound invader and anti-invader form an inert complex whose concentration increases during this experiment). Error bars are the standard error of the mean derived from bootstrapping data from a single experimental replicate. Scale bars are 10 μm.

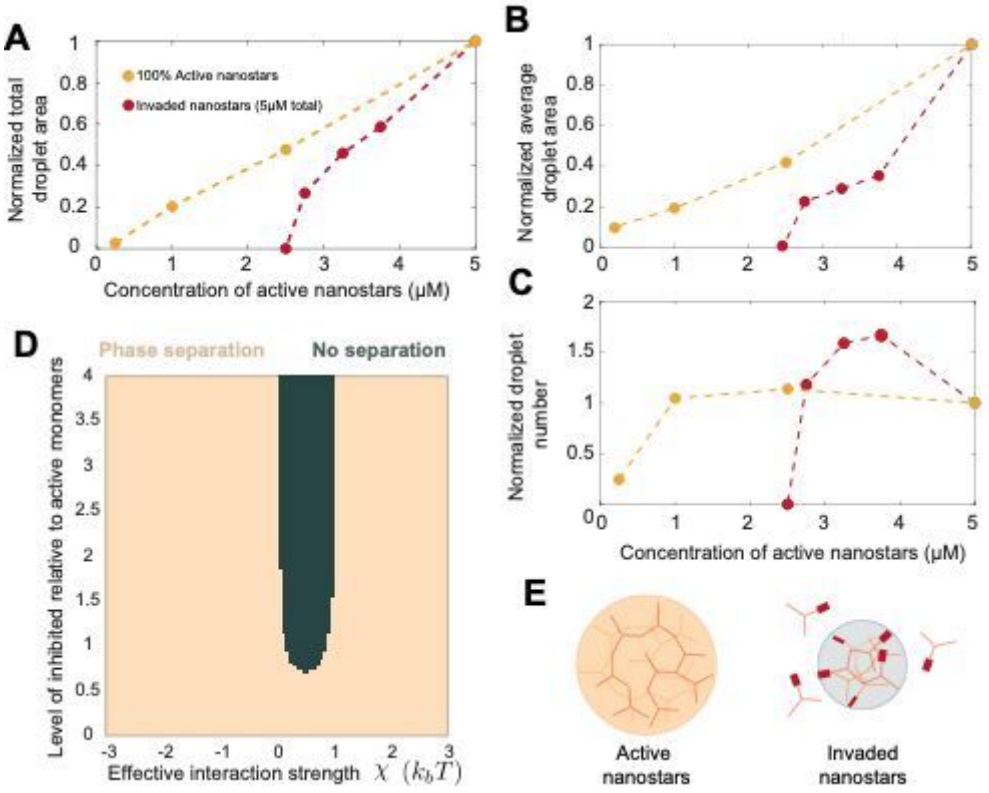

Figure 3

Invasion allows for efficient control of phase separation. *A) Normalized total condensate area measured 30 minutes after anneal versus level of active nanostars in the presence or absence of invader. B) Normalized average droplet area, and C) Normalized average droplet number, measured 30 minutes after anneal. D) Computational phase diagram (SI Section 4.1) illustrating the existence of a range of interaction strengths between active and inactive monomers in which phase separation is suppressed at ~.6 ratio of inactive/active monomers. E) Schematic representation of the invasion process causing a reduction of valency of individual nanostars. Invaded nanostars can still interact with other active nanostars, limiting their capacity to form condensates. Normalization is done relative to area (average or total) measured at 5μM nanostar; data are from a single experimental replicate for each condition.*

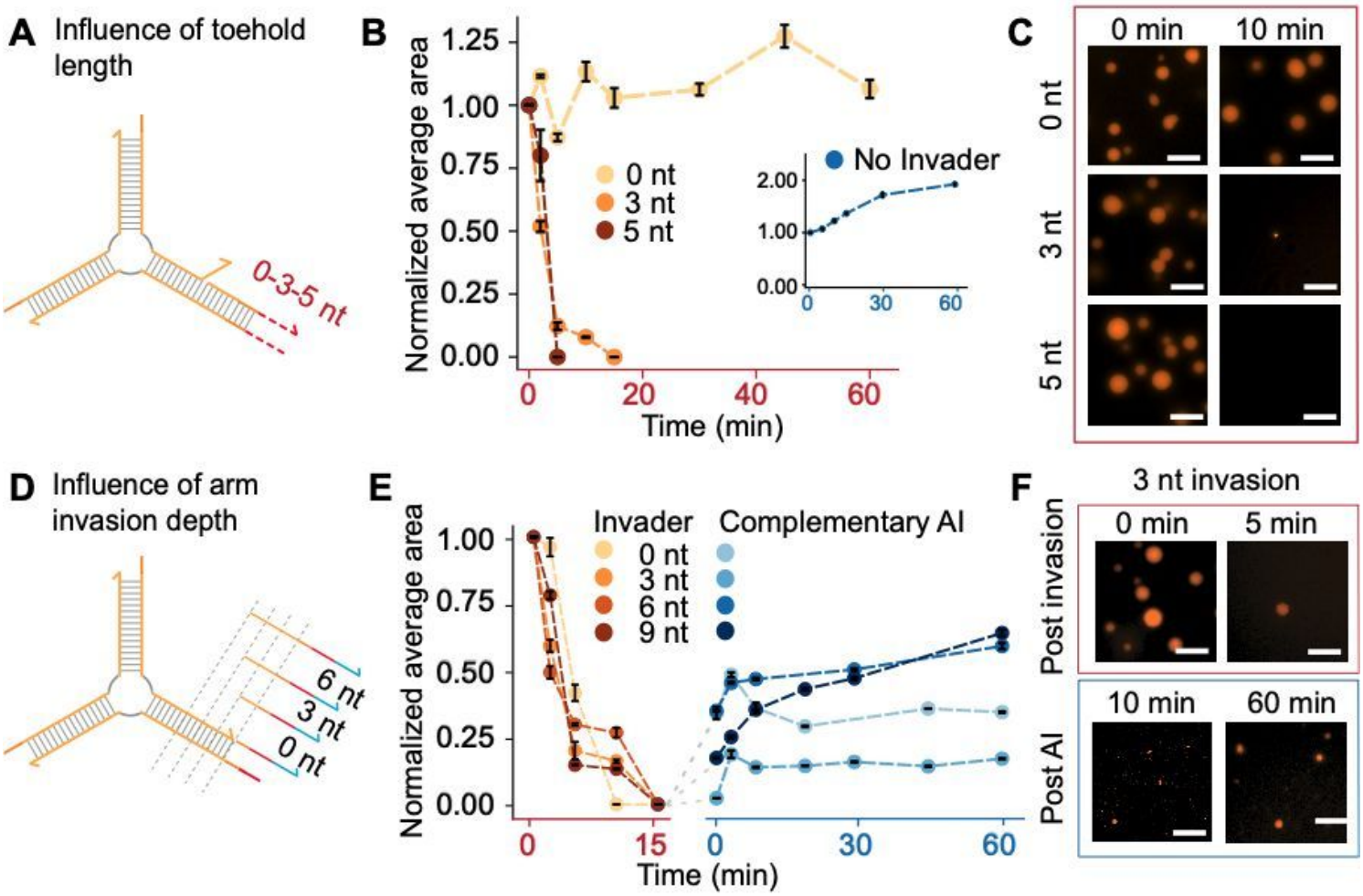

Figure 4

Changing the invasion and anti-invasion interaction domains affects the droplet response.

A) Schematic representation of the difference in the invader-nanostar bond based on the length of the toehold region present. B) Normalized average area of droplets with different toe-hold lengths for invasion. Inset: Normalized average area of droplets without the presence of any invader species. Invaders = 1X. C) Microscopic images show the change in the droplets before and after 10 mins of invader addition. D) Schematic representation of the difference in the invader-nanostar bond based on the depth of the invasion domain. E) Normalized average area of droplets after addition of invaders with depths from 0-9 nucleotides and the after the addition of anti-invaders which are complementary to the specific invaders. Invaders = 0.5X, AI = 0.5X. F) Microscopic images show the change in the droplets in the sample with an invasion depth of 3 nucleotides and their regrowth post anti-invasion. Error bars are the standard error of the mean derived from bootstrapping data from a single experimental replicate. Scale bars are 10 μm.

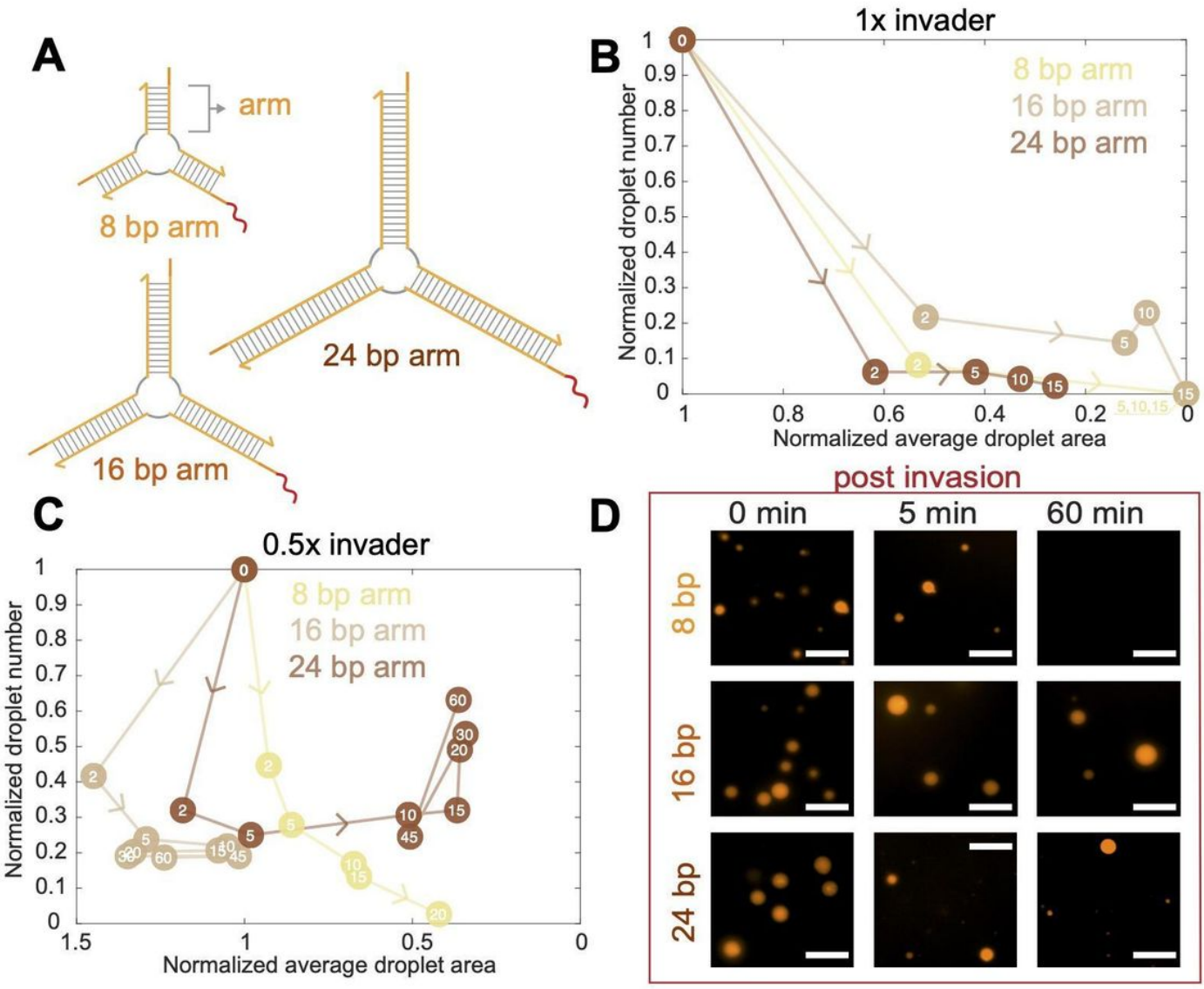

Figure 5

Dissolution kinetics of droplets produced by nanostars of different size *A) Schematic representation of the nanostars with different arm length and same sticky-end domain. B) With 1X invader, normalized droplet number and normalized average area decreases to zero within 15 minutes. C) With 0.5X invader, normalized droplet number and normalized average area gradually decreases to zero for the 8 bp variant but not for the 16 and 24 bp variants. D) Microscopic images show the change in the droplets before and after 10 mins of invader addition in different designs. Scale bars are 10 μm.*

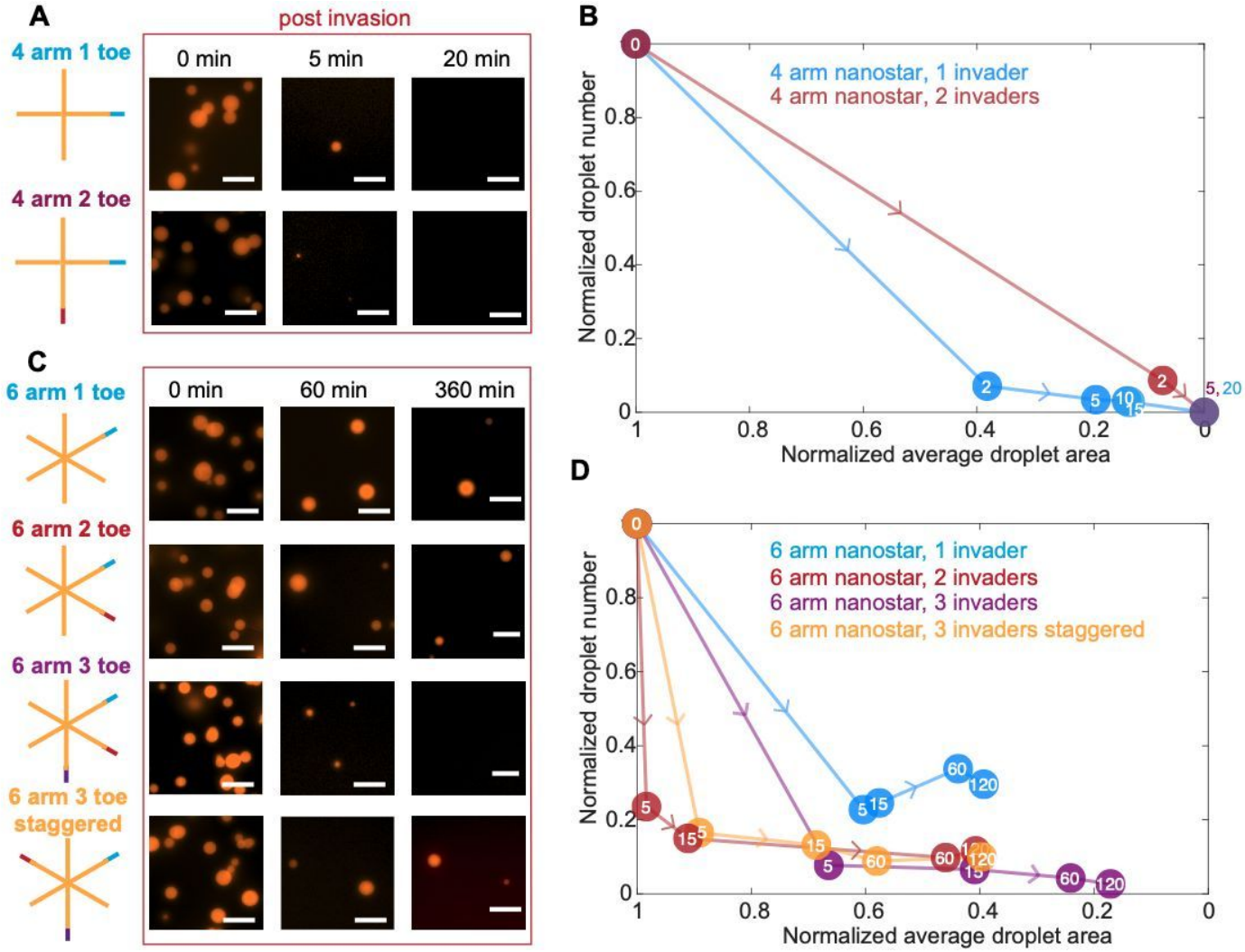

Figure 6

Controlling the valency of nanostars via distinct toeholds *A) Schematic representation of the Nanostars with 4 arms, and one or two toeholds for invasion. Microscopic images show the change in the droplets after invader addition corresponding to each toehold region present on the variant (each Inv = 1X). B) Normalized droplet area for the condensates formed by 4 arm nanostar with two invasion points decreases more rapidly than those formed by 4 arm nanostar with one invasion point. Normalized droplet number for 4 arm nanostar design with two invasion points reaches zero within 5 mins of invader addition. C) Schematic representation of the nanostars with 6 arms and one, two or three toeholds for invasion. Three toeholds are placed next to each other in the adjacent variant and in an alternating pattern in the staggered variant. Microscopy images show the change in the droplets after invader addition corresponding to each toehold region present on the variant (each Inv = 1X). D) Normalized droplet area and normalized droplet number for the 6 arm nanostar design with three adjacent invasion points reaches zero after 120 mins of invader addition. The 6 arm nanostar design with three staggered invasion points behaves similarly to 6 arm nanostar with two invasion points, whereas 6 arm nanostar with one invasion point does not dissolve. Scale bars are 10 μm.*

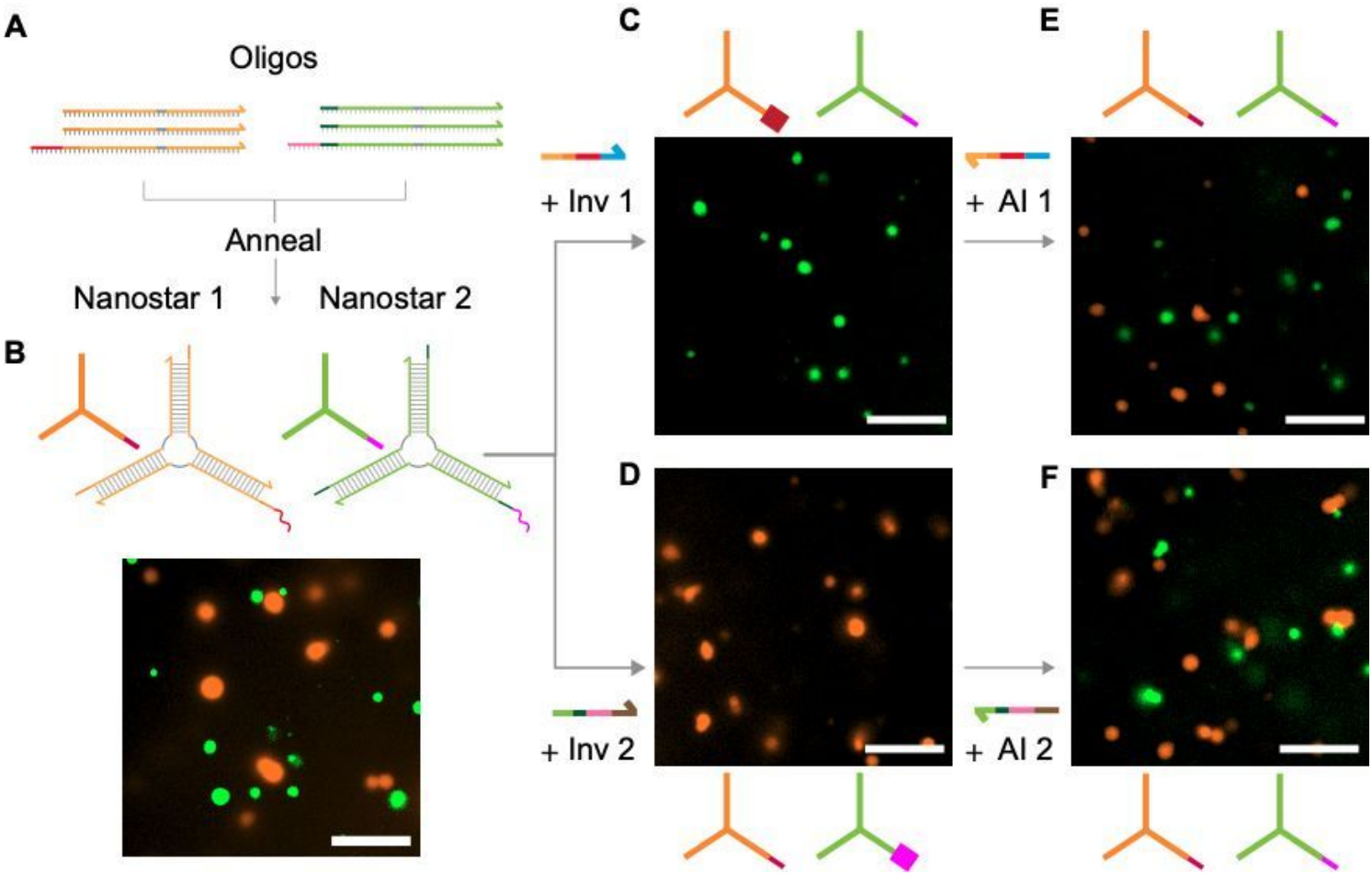

Figure 7

Sequence specific dissolution and regrowth of distinct condensates *A and B) Orthogonal DNA strands can be annealed to form orthogonal DNA nanostars that do not interact. B) Nanostar 1, labeled with cy3, is represented in orange and nanostar 2, labeled with FAM, is represented in green. C) and D) Invaders specific to either Nanostar 1 or Nanostar 2 selectively inhibit their capacity to phase separate while leaving the other unaffected, as shown by microscopy images. E) and F) Respective Anti-Invaders for each design reactivate their capacity to phase separate again. Microscopy images were taken 5 mins after the addition of the respective invader or anti-invader strands. Inv and AI = 1X. Scale bars are 10 µm.*

Supplementary Files

This is a list of supplementary files associated with this preprint. Click to download.

- SIfileBiochemicalControlOfDNACondensation.docx